

Finally, we assume the volume dependence of W is given by Heine's²³ results

$$\frac{\partial \ln W}{\partial \ln V} = -\frac{5}{3} \quad (5)$$

Using the above results, Eqs. (3)–(5), the volume dependence of \bar{I} , Eq. (2), is¹²

$$\frac{\partial \ln \bar{I}}{\partial \ln V} = \frac{5}{3} \frac{I}{I_b}, \quad (6)$$

which is independent of β and γ and where here I_b is assumed independent of volume. For the density of states of the form given by Eq. (4), it can be shown that $T_F \sim W$, and hence from Eq. (5), $\partial \ln T_F / \partial \ln V = -\frac{5}{3}$. Using Eqs. (1), (2), (5), and (6) the volume dependence of T_c becomes

$$\begin{aligned} \frac{\partial \ln T_c}{\partial \ln V} &\equiv \Gamma \\ &= -\frac{5}{3} + \frac{5}{6} (\bar{I} - 1)^{-1} (I/I_b). \end{aligned} \quad (7)$$

In terms of pressure, Eq. (7) can be written as

$$\frac{\partial T_c}{\partial P} = \frac{5}{3} \kappa T_c - \frac{5}{6} \kappa \frac{I}{I_b} \frac{T_F^2}{T_c}, \quad (8)$$

where κ is the volume compressibility and we have used Eq. (1).

We shall now show how pressure measurements of T_c can be used to determine a maximum value for \bar{I} and a minimum value for T_F . The maximum value that I can have is the bare exchange value I_b ; thus, the maximum value for the ratio I/I_b is one. Hence, the experimental value of Γ can be used to determine the maximum values of \bar{I} . From Eq. (7) we have

$$\bar{I}_{\max} = 1 + \frac{5}{6} (\Gamma + \frac{5}{3})^{-1}. \quad (9)$$

Then using values for \bar{I} obtained from Eq. (9) we can obtain a minimum value for T_F using Eq. (1).

For weak itinerant-electron FM's $\bar{I} \gtrsim 1.0$ and for weak electron-correlation effects $I/I_b \cong 1.0$, the second term in Eq. (7) is dominant, and from Eq. (8) we have $\partial T_c / \partial P \sim -1/T_c$. Examples of weak itinerant-electron FM's are the Fe-Ni, Fe-Pt, and Fe-Pd Invar alloys where it has been experimentally observed that $\partial T_c / \partial P \cong -\text{const}/T_c$.²⁴ For strong itinerant-electron FM's $\bar{I} > 1$ and for strong correlation effects $I/I_b < 1$ such that the first term in Eq. (7) is dominant, and from Eq. (8) we have $\partial T_c / \partial P \sim T_c$. An example of a strong itinerant-electron FM is Ni, where it is found that $\partial T_c / \partial P = \frac{5}{3} \kappa T_c \cong 0.68 \text{ }^\circ\text{K/kbar}$ in good agreement with experimental values of $0.32\text{--}0.42 \text{ }^\circ\text{K/kbar}$.⁹ It is noteworthy that in the limit of weak itinerant-electron FM and for large Γ such that $|\Gamma| \gg \frac{5}{3}$ and neglecting the volume dependence of I_b , the results of this paper reduce to the results given previously by Wohlfarth and Bartel.¹²

The localized and the itinerant, or collective,

descriptions of magnetic electrons have been investigated by Goodenough.²⁵ He considered the case of one d electron per relevant d orbital which corresponds to a half-filled band or to a half-filled localized orbital, and the magnetic order is antiferromagnetic (AFM). In the absence of competing exchange interactions, the Néel temperature T_N for localized-electron AFM increases with the transfer integral b since the exchange interaction is proportional to b^2 ; whereas, it has been shown that T_N for a band AFM decreases with increasing bandwidth^{25,26} where the bandwidth is proportional to b . Goodenough concludes that the magnetic moment and T_N should vary continuously in going from a localized to a band description. We expect b to increase with increasing pressure; hence, we expect that for the localized electron description T_N should increase with increasing pressure, and for the itinerant description T_N should decrease with increasing pressure.²⁶ Furthermore, we expect that the general arguments for an AFM apply to the FM case of interest here. The observed decrease in the FM-to-PM transition temperature in the $\text{MnAs}_x\text{Sb}_{1-x}$ compounds suggests that the itinerant-electron description is the appropriate one. Although these compounds are anisotropic, the isotropic model discussed in this paper describes the pressure effects quite well.

2. Analysis of Experimental Results

In Fig. 6, $\partial T_c / \partial P$ is plotted as a function of T_c for the $\text{MnAs}_x\text{Sb}_{1-x}$ solid solutions in the concentration range $0 \leq x \leq 0.8$. For comparison, the Fe-Ni, Fe-Pd, and Fe-Pt Invar alloy data of Wayne and Bartel²⁴ are included. Similar to the Invar alloys, we observe a T_c^{-1} type of behavior as predicted by Eq. (8) when the second term in Eq. (8) dominates.

The volume derivative of T_c is calculated from $\partial T_c / \partial P$ where the compressibility for the solid solutions was obtained by a linear extrapolation between the values of $(2.5 \pm 0.5) \times 10^{-3} \text{ kbar}^{-1}$ for MnSb²⁷ and $4.55 \times 10^{-3} \text{ kbar}^{-1}$ for MnAs.¹ The values for Γ are given in Table I. We observe that the values of Γ increase with increasing As concentration and that the magnitude of Γ is of the same order of magnitude as the first term in Eq. (7). In previous works on the Invar alloys^{11,12} and ZrZn_2 ,⁹⁻¹² it was observed that $\Gamma \gg \frac{5}{3}$ and so the first term of Eq. (7) could be neglected. In the case of the $\text{MnAs}_x\text{Sb}_{1-x}$ solid solutions, this factor of $\frac{5}{3}$ must be included in any calculation of band parameters.

In Table I, we give the results of the calculation of \bar{I}_{\max} from Eq. (9) for the solid solutions $0 \leq x \leq 0.80$. The quoted error in the compressibility for MnSb will introduce an uncertainty of ± 0.03 in the value for \bar{I}_{\max} . We observe that \bar{I}_{\max} decreases with increasing As concentration. According to Wohl-

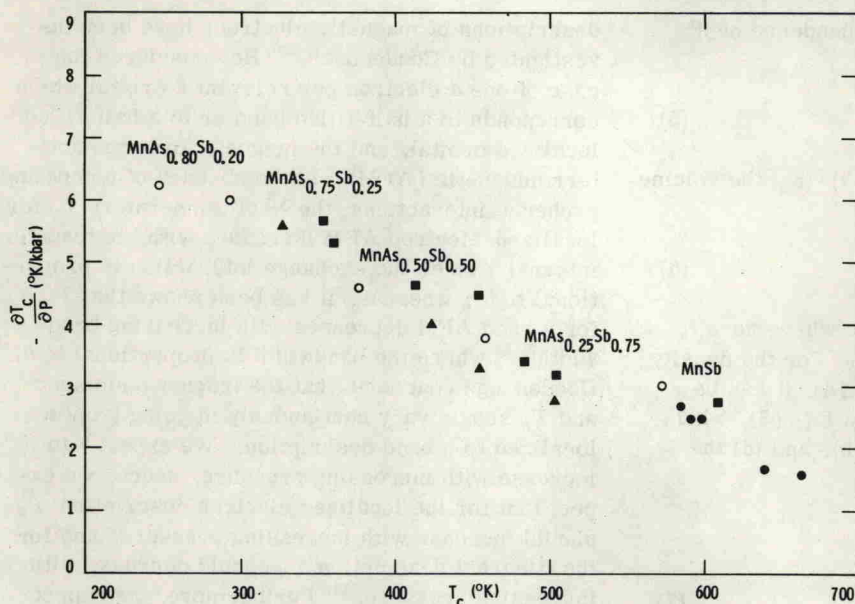


FIG. 6. A comparison of $\partial T_c/\partial P$ -vs- T_c plots for various alloy systems. Open circle, $\text{MnAs}_x\text{Sb}_{1-x}$; triangles Fe-Pt; solid circle, Fe-Pd; and square, Fe-Ni.

farth's²⁸ classification, these values of \bar{I}_{\max} indicate that MnSb is approaching a strong itinerant FM, and the solid solutions are becoming weaker itinerant FM's with increasing As concentration. These values of \bar{I}_{\max} for the $\text{MnAs}_x\text{Sb}_{1-x}$ solid solutions are comparable with the values for the Invar alloys.²⁹

From Eq. (1), and using the value of \bar{I} and T_c for MnSb from Table I, we calculate $T_F = 1380^\circ\text{K}$. Thus for MnSb we see that $T_c \approx 0.4T_F$ which indicates the Sommerfeld expansion is converging; however, the convergence is slower than one would desire. For the materials with $x > 0$, the convergence is more rapid than for $x = 0$.

Using Eqs. (1)–(4), we can express T_c as a function of the bandwidth W where we assume $T_F \sim W$. Then using the value of $T_c = 572^\circ\text{K}$ and the value of \bar{I}_{\max} from Table I for MnSb, we can calculate T_c as a function of W . The results of these calculations are shown in Fig. 7. These results are independent of the value of I/I_b ,³⁰ but do not include effects of any volume dependence of I_b . Note the critical bandwidth such that for $W/W_0 \geq 1.206$ we do not have FM order, and note the quadratic dependence of T_c on W for $W/W_0 \leq 1.206$. Using the available x-ray data³¹ to estimate W/W_0 and using the experimental values for T_c we show, in Fig. 7, the experimental results of T_c as a function of W/W_0 . For $x = 0.25$ we calculate $T_c = 474^\circ\text{K}$ and $\bar{I} = 1.110$ in fair agreement with the experimental values. For the solid solutions $x > 0.25$ the agreement is only qualitative. This disagreement is not too surprising because of the large differences in unit-cell volumes for the various compositions. For these large volume differences one might expect

significant changes in the crystal-field splittings, and consequently significant changes in the electronic wave functions. Any volume dependence of I_b would modify the results shown in Fig. 7. Lacking specific-heat, susceptibility, and magnetostriction data for these materials, we cannot determine $N(\epsilon_F)$, I , I_b , and any volume dependence of I_b individually. In addition, as we shall point out below, we expect rather large electron-lattice and exchange-striction interactions for these materials, particularly for the solid solutions $x \geq 0.80$. Electron-lattice and exchange-striction effects have not been included in the calculations displayed in Fig. 7.

Sirota and Vasilev⁴ have observed a Curie-Weiss type of behavior in the PM region for MnSb, with a Curie constant, $C_M = 1.3 \text{ emu mole}^{-1} \text{Oe}^{-1} \text{K}^{-1}$. According to the itinerant FM model of Wohlfarth⁹ the susceptibility in the temperature region $T_F \gg T > T_c$ and for $T - T_c$ can be written as $\chi \approx \chi_0 T_c \times (T - T_c)^{-1}$ which is a Curie-Weiss type of behavior where the Curie constant C_M is given by $C_M = \chi_0 T_c$. The quantity χ_0 is proportional to $N(\epsilon_F)(\bar{I} - 1)^{-1}$.⁹ For MnSb, χ_0 can be calculated to give $\chi_0 = 0.227$

TABLE I. Curie temperature T_c , $\Gamma \equiv \partial \ln T_c / \partial \ln V$, and \bar{I}_{\max} , as calculated from Eq. (9), for various solid solutions of $\text{MnAs}_x\text{Sb}_{1-x}$ in the second-order region.

x (at. % As)	T_c	Γ	\bar{I}_{\max}
0.00	572	2.38	1.206
0.25	458	2.97	1.180
0.50	375	3.63	1.157
0.75	292	5.18	1.122
0.80	247	6.20	1.106